RSC Advances

PAPER

View Article Online
View Journal | View Issue

Cite this: *RSC Adv.*, 2021, **11**, 22598

Synergic effects between boron and nitrogen atoms in BN-codoped $C_{59-n}BN_n$ fullerenes ($n = 1$–3) for metal-free reduction of greenhouse N_2O gas†

Mehdi D. Esrafili, *[a] Adnan Ali Khan [bc] and Parisasadat Mousavian[ad]

The geometries, electronic structures, and catalytic properties of BN-codoped fullerenes $C_{59-n}BN_n$ ($n = 1$–3) are studied using first-principles computations. The results showed that BN-codoping can significantly modify the properties of C_{60} fullerene by breaking local charge neutrality and creating active sites. The codoping of B and N enhances the formation energy of fullerenes, indicating that the synergistic effects of these atoms helps to stabilize the $C_{59-n}BN_n$ structures. The stepwise addition of N atoms around the B atom improves catalytic activities of $C_{59-n}BN_n$ in N_2O reduction. The reduction of N_2O over $C_{58}BN$ and $C_{57}BN_2$ begins with its chemisorption on the B–C bond of the fullerene, followed by the concerted interaction of CO with N_2O and the release of N_2. The resulting OCO intermediate is subsequently transformed into a CO_2 molecule, which is weakly adsorbed on the B atom of the fullerene. On the contrary, nitrogen-rich $C_{56}BN_3$ fullerene is found to decompose N_2O into N_2 and O* species without the requirement for activation energy. The CO molecule then removes the O* species with a low activation barrier. The activation barrier of the N_2O reduction on $C_{56}BN_3$ fullerene is just 0.28 eV, which is lower than that of noble metals.

Received 24th May 2021
Accepted 21st June 2021

DOI: 10.1039/d1ra04046d

rsc.li/rsc-advances

1. Introduction

The increase in atmospheric concentration of greenhouse gases is among the most serious threats to our planet.[1,2] These species are able to trap solar energy and emit it within the thermal infrared range. Although greenhouse gases are naturally present in the Earth's atmosphere, human activities like agriculture, fuel combustion and industrial processes have led to a continual build-up of these heat-trapping gases, hence intensifying the greenhouse effect. Nitrous oxide (N_2O) is a long-lived greenhouse gas which is recognized as a main contributor to global warming and climate change.[3] The other concern about N_2O is that it is unstable in the stratosphere and can be easily decomposed into nitrogen oxides (NO_x). These NO_x are able to interact with the ozone molecule, leading to the ozone layer depletion.[3,4] Therefore, considerable efforts have been made to find practical solutions to decrease or remove harmful N_2O molecules from the atmosphere.[5–8] For instance, many theoretical calculations and experimental studies have focused on the catalytic reduction of N_2O by carbon monoxide (CO) as an efficient and possible solution for removing of N_2O.[6,9–11] Transition-metal (TM) catalysts including cations,[12,13] clusters[14] and those finely isolated on supports[15,16] have been also frequently used as durable and efficient materials to accelerate this process. In addition, some TM-free catalysts like B-,[17] Al-(ref. 18) or Si-doped graphene[19,20] have also attracted increasing attention to tackle the serious environmental problems caused by N_2O emission.

In recent decades, carbon-based nanoparticles like fullerenes, nanocones, nanotubes and graphene have drawn a lot of attention in various fields of chemistry and materials science due to their exceptional physicochemical properties, unique specific area and low cost.[21–27] Apart from these characteristics, theoretical studies[28–31] have proven that the chemical doping with heteroatoms can drastically improve the electronic structure of carbon nanomaterials. For instance, earlier studies[32,33] have pointed out that the chemical doping of C_{60} fullerene with B atoms can substantially enhance its catalytic properties in the oxygen reduction reaction (ORR) due to activation of adsorbed O_2 molecules. Recently, Chen and coworkers[34] have identified that the $C_{59}B$ fullerene could serve as a superior and robust catalyst for CO oxidation. Since the boron atom has a lower electronegativity than carbon (2.0 *vs.* 2.5 based on Pauling's scale), the introduction of a boron atom can provide an active catalytic center in C_{60} to capture O_2 molecules. Likewise, N-doping has also been suggested as a useful strategy for tuning the electronic structure and properties of carbon-based nanomaterials.[35–38] For example, graphene

[a]*Department of Chemistry, Faculty of Basic Sciences, University of Maragheh, P. O. Box 55136-553, Maragheh, Iran. E-mail: esrafili@maragheh.ac.ir*

[b]*Centre for Computational Materials Science, University of Malakand, Chakdara, Pakistan*

[c]*Department of Chemistry, University of Malakand, Chakdara, Pakistan*

[d]*Department of Chemistry, Azarbaijan Shahid Madani University, Tabriz, Iran*

† Electronic supplementary information (ESI) available. See DOI: 10.1039/d1ra04046d

layers doped with nitrogen atoms are among the most studied systems with novel and superior catalytic activity in different chemical reactions.[39–42] In addition to large electronegativity, which causes a positive charge over the nearest carbon atoms, the presence of nitrogen atoms can bring an asymmetric spin density in carbon nanomaterials. Therefore, N-doped carbon nanomaterials have been frequently exploited as metal-free catalysts in various chemical reactions like ORR,[43–45] CO oxidation[46–48] and NO reduction.[49]

Some experimental investigations and theoretical calculations have claimed that B and N codoping of carbon-based nanomaterials can offer further intriguing opportunities to realize new metal-free catalysts due to the synergistic effects between B and N atoms.[50–53] For instance, Wang *et al.*[54] prepared BN-codoped graphene for the ORR with superior catalytic ability comparable with those of commercial Pt-based catalysts. In addition to such high catalytic performance, a combined experimental and theoretical work has also found the BN codoping can provide 100% selectivity for the ORR process *via* the four-electron pathway.[55] Density functional theory (DFT) computations also confirmed that the active graphitic BN_3 sites could improve the O_2 (ref. 56 and 57) and N_2O adsorptions[17] in the BN-codoped graphene. Extensive studies have also proven that the presence of BN moieties in carbon fullerenes can provide active sites for sensing toxic gas molecules.[53,58] Furthermore, the difference in electronegativity between B, C and N atoms can polarize the inert carbon-π electron density in these systems, rendering them as excellent substrates for Li-ion batteries[59,60] and H_2 storage.[61] However, little is yet known about the mechanism of N_2O reduction and the synergic effects between B and N atoms in the BN-codoped fullerenes.

C_{60} fullerene, on the other hand, may trap atoms and small molecules to form stable endohedral complexes with tremendous potential uses as superconductors, drug delivery systems, and molecular reactors.[62–64] For example, noble gases (Ng = He, Ne, Ar, Kr, Xe) can be introduced into the C_{60} by applying high temperatures and pressure to a mixture of fullerenes and the target Ng, hitting fullerenes with accelerated ions, or other techniques.[65] DFT computations have demonstrated that encapsulating a Ng atom in the C_{60} fullerene can stabilize the system due to the coupling the electronic states of the encapsulated atom with those of fullerene C atoms.[66] Bühl *et al.*[67] found that the negative interaction energies between endohedral He to Xe atoms and C_{60} increase with the Ng size (Xe > Kr > Ar > Ne > He) owing to enhanced dispersion interactions. Sola and coworkers[68] examined the activation energies of the [4+2] Diels–Alder cycloaddition processes in free and Ng endohedral Ng@C_{60} systems (Ng = He–Xe), and found that the Ng atom has only a little effect on the activation energy of this reaction. According to Bil *et al.*,[69] the addition of an endohedral Ng atom could influence the ozone ring-opening process in Ng@$C_{70}O_3$, but has no effect on the relative stability of the $C_{70}O_3$ isomers. Based on these findings, one might ask whether adding an endohedral Ng atom to BN-codoped C_{60} fullerenes improves the N_2O reduction reaction on these systems.

In the present study, by employing first-principles calculations, we focus on the mechanisms of N_2O reduction over $C_{59-n}BN_n$ fullerenes (n = 1–3). We show that the successive substitution of N atoms around a pre-doped boron atom can substantially enhance the tendency of C_{60} fullerene to capture N_2O molecule. In particular, because of curvature effects, the chemisorption of a N_2O molecule is found to be stronger than that of on the BN-codoped graphene. Due to distinct electronic structure and sizable charge-transfer, the nitrogen-rich $C_{56}BN_3$ fullerene exhibits highest activity for the N_2O reduction. Our results propose that C_{60} fullerenes with a small content of B and N atoms provide exceptional catalytic performance for reduction of N_2O at low-temperatures.

2. Theoretical details

To explore N_2O reduction on $C_{59-n}BN_n$ fullerenes, we implemented spin-polarized DFT calculations with the Perdew–Burke–Ernzerhof (PBE)[70] functional in combination with an all-electron double-ξ numerical basis set involving polarization functions (DNP). The dispersion interactions were corrected with the DFT+D2 scheme of Grimme.[71] All the simulations were done in a 25 × 25 × 25 Å cubic box, with a gamma point for the summation in the Brillouin zone. The BN-codoped fullerenes were obtained *via* replacement of C atom(s) around the B atom of $C_{59}B$ with the N atom(s). The Hirshfeld method was adopted for the population analysis. To search transition states (TS), the complete LST/QST method was employed. All the calculations were done with the DMol^3.[72,73]

The relative stability of BN-codoped fullerenes was evaluated by formation energy (E_{form}), defined as

$$E_{form} = E_{C_{59-n}BN_n} - E_{C_{60}} + (n+1)\mu_C - (\mu_B + n\mu_N) \quad (1)$$

in which n is the number of doped nitrogen atom; while the $E_{C_{59-n}BN_n}$ and $E_{C_{60}}$ are the energies of doped and undoped C_{60} fullerenes, respectively. The μ_B and μ_N are the chemical potential of B and N atoms calculated as the energy of C and N atoms in C_{60} and N_2 molecules, respectively. In addition, the durability of $C_{59-}nBNn$ fullerenes was assessed by binding energy of the B atom in these systems obtained as

$$E_{bind} = E_{C_{59-n}BN_n} - E_B - E_{defective} \quad (2)$$

where $E_{C_{59-n}BN_n}$ is the energy of BN-codoped structure, E_B is the energy of a single B atom and $E_{defective}$ is the energy of single-vacancy defective $C_{59-n}BN_n$ fullerenes (Fig. S1 of ESI†).

The adsorption energies (E_{ad}) of N_2O and CO were obtained as the difference between the total energy of the resulting complex ($E_{complex}$) and sum of the energy of isolated reactant (E_X) and fullerene ($E_{fullerene}$):

$$E_{ad} = E_{complex} - (E_X + E_{fullerene}) \quad (3)$$

By this equation, a negative E_{ad} value shows that the resulting complex would be stable and its formation is a thermodynamically facile process. To consider the temperature and entropic effects, the adsorption Gibbs free energy changes (ΔG_{ad}) were obtained at T = 298.15 K and P = 1 atm, according to the following equation:

$$\Delta G_{ad} = (\varepsilon_{complex} + G_{corr,complex}) - [(\varepsilon_X + G_{corr,X}) + (\varepsilon_{fullerene} + G_{corr,X\ fullerene})] \quad (4)$$

where $\varepsilon_{complex}$, ε_X and $\varepsilon_{fullerene}$ are the zero-point corrected energies of the species defined in the eqn (3). The G_{corr} term is the thermal and entropic correction of the energy defined as:

$$G_{corr} = H_{corr} - TS_{tot} = (E_{tot} + k_B T) - TS_{tot} \quad (5)$$

here the k_B is the Boltzmann constant. The E_{tot} and S_{tot} are the internal thermal energy and entropy, respectively. A negative ΔG_{ad} value shows the adsorption process is thermodynamically facile at $T = 298.15$ K and $P = 1$ atm.

We also investigated the nature of the interactions in N_2O and CO adducts of $C_{59-n}BN_n$, which seems to be affected by the composition of fullerene.[74,75] The quantum theory of atoms in molecules (QTAIM)[76] was used here to investigate the nature of interactions between fullerenes and adsorbed N_2O or CO molecules. QTAIM is based on topological analysis of electron density, which determines the nature of a chemical bond by analyzing electron density at a specific point between interacting atoms, known as the bond critical point (BCP).[76] Although the gradient of electron density at the BCP is nearly zero, the electron density (ρ_{BCP}) and its Laplacian ($\nabla^2\rho_{BCP}$) can provide valuable information about the nature of the interaction. In QTAIM, a covalent interaction is distinguished by a large ρ_{BCP} and a negative $\nabla^2\rho_{BCP}$, whereas a closed-shell interaction is identified by a small ρ_{BCP} and a positive $\nabla^2\rho_{BCP}$. In addition, $\nabla^2\rho_{BCP}$ and total electronic energy density at the BCP (H_{BCP}) may be used to assess the degree of covalency of the interaction between two atoms.[77] That is, for a covalent interaction, $\nabla^2\rho_{BCP} < 0$ and $H_{BCP} < 0$, for an electrostatic interaction, $\nabla^2\rho_{BCP} > 0$ and $H_{BCP} > 0$, and for a partially covalent interaction, $\nabla^2\rho_{BCP} > 0$ and $H_{BCP} < 0$. The AIM2000 (ref. 78) was used to perform the QTAIM analyses in this study, using the PBEPBE/6-31++G** wave functions generated by the Gaussian 09 software package.[79]

3. Results and discussion

3.1. $C_{59-n}BN_n$ fullerenes

Fig. 1 depicts the relaxed atomic structures of BN-codoped fullerenes $C_{59-n}BN_n$ (n = 1–3), as well as the molecular electrostatic potentials (MEP) and total density of states (TDOS) plots. The equilibrium geometry and electrical structure of $C_{59}B$ heterofullerene and pure C_{60} are also presented to help understand the effect of B and N doping. A carbon atom of pure C_{60} is substituted with a boron impurity to produce $C_{59}B$. The BN-codoped $C_{58}BN$, $C_{57}BN_2$ and $C_{56}BN_3$ structures were then constructed by successively substituting the carbon atoms around the B atom in $C_{59}B$ with the N atom. Though the close cage structure of C_{60} is retained in all the systems, the substitution of C atoms with B and N makes some distortions in the vicinity of the dopant atoms. According to Table 1, the formation energy (E_{form}) of $C_{59}B$ is −5.23 eV, which is in agreement with those reported by other studies.[80] This negative E_{form} value suggests that a B atom may be simply incorporated within the C_{60} structure and the formation of $C_{59}B$ would be thermodynamically feasible at normal temperatures. The newly formed B–C bonds distances are calculated to be 1.52 and 1.55 Å, which match reasonably with those previous studies.[80–82] Table 1 also lists the E_{form} values of BN-codoped structures. It is seen that as the C atoms around the B in $C_{59}B$ is substituted with the N atoms, the E_{form} of the fullerene increases to −6.13 ($C_{58}BN$), −6.66 ($C_{57}BN_2$) and −6.63 eV ($C_{56}BN_3$). This implies that the substitutional nitrogens increase the durability and stabilization of $C_{59}B$ fullerenes, and the BN codoping of C_{60} is more energetically desirable than the doping of a B atom. The latter can be explained by the donor–acceptor interaction between the vacant orbital of B and lone-pair electrons of the added N atoms. From the E_{form} values, this donor–acceptor interaction increases as $C_{57}BN_2$ > $C_{56}BN_3$ > $C_{58}BN$. The average B–N bond distances of $C_{58}BN$, $C_{57}BN_2$ and $C_{56}BN_3$ are calculated to be 1.50, 1.46 and 1.44 Å, respectively, which are about 6, 3 and 2% longer than the B–C bond of $C_{59}B$. It is evident from Table 1 that the binding energy (E_{bind}) of the B atom at the vacancy site also varies with the number of nitrogen dopants around it. Interestingly, the E_{bind} values of B in the BN-codoped fullerenes are smaller than that of $C_{59}B$, which can be related to the larger bond formation energy of B–C (≈ -4.65 eV) than B–N (≈ -4.04 eV).[83] Nevertheless, the large negative E_{bind} values indicate that the B atom in $C_{59-n}BN_n$ fullerenes cannot be easily diffused and hence these systems can remain as a stable catalyst even at high temperatures.

Since N_2O molecule is a polar molecule, it is expected that its adsorption and subsequent catalytic reduction are directly related to charge distribution of the catalyst surface. Hence, we provided the MEP isosurfaces of $C_{59}B$ and $C_{59-n}BN_n$ fullerenes in Fig. 1. For the all systems studied, there is a positive electrostatic potential region developed on the B atom, indicating the possibility of this site to interact with nucleophilic species. As the electronegativity of N is greater than that of B, hence, $C_{56}BN_3$ indicates the largest electrostatic potential among the $C_{59-n}BN_n$ systems. From Fig. 1, one can see that there is a quite small potential on the B atom of $C_{58}BN$ which is because of the charge transfer from the lone-pair of N atom into unfilled orbital of B. This builds up a sizable electron density in the region between the B and N atoms as evidenced from the corresponding MEP isosurface. However in the case of $C_{57}BN_2$ and $C_{56}BN_3$, the addition of second and third N atoms withdraws the electron density around the B atom and hence induces a large positive electrostatic potential over the B atom. These results are fully consistent with the Hirshfeld analysis results in Table 1, in which the substitution of first N atom has a negligible influence on the charge of the B atom. However, the incorporation of second and third N atoms induces a larger positive charge over the B atom, a phenomenon which is beneficial for the N_2O adsorption. Accompanied with these charge redistributions, the electronic structure of $C_{59-n}BN_n$ systems is also regulated as the number of involved nitrogen atoms grows. From the TDOS maps in Fig. 1, it is seen that the successive

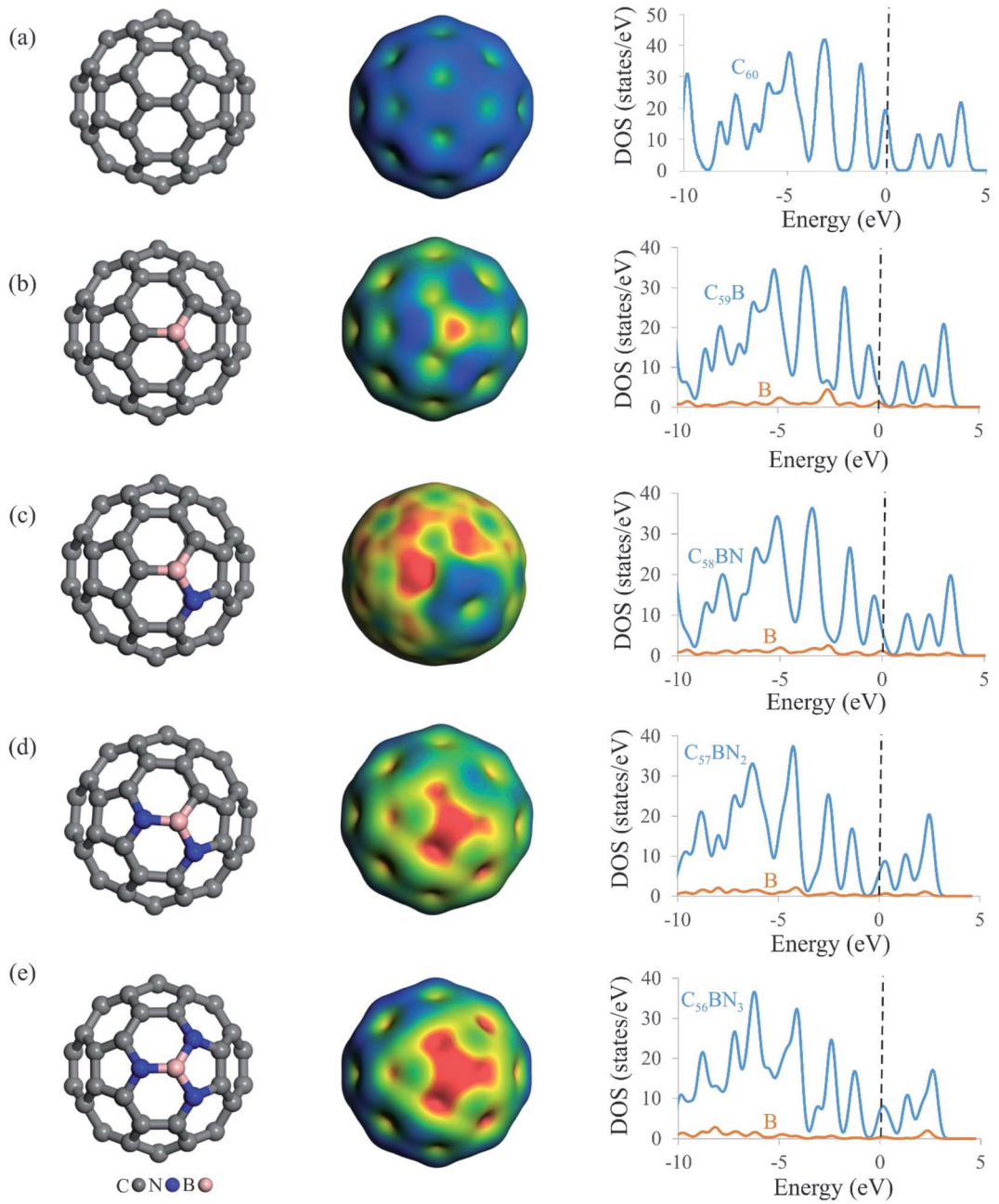

Fig. 1 Local atomic structures (left) molecular electrostatic potential isosurfaces (MEP, middle) and TDOS plots (right) of (a) C_{60}, (b) $C_{59}B$, (c) $C_{58}BN$, (d) $C_{57}BN_2$ and (e) $C_{56}BN_3$. The dashed line in TDOS plots shows the Fermi level. The color range in the MEP maps is from blue (more negative = −0.001 a.u.) to red (more positive = 0.078 a.u.).

Table 1 The formation energy (E_{form}, eV), binding energy of B atom at the single-vacancy site (E_{bind}, eV), and Hirshfeld charge of the B atom (q_B, $|e|$) in the bare $C_{59-n}BN_n$ fullerenes

Fullerene	E_{form}	E_{bind}	q_B
$C_{59}B$	−5.23	−8.74	0.09
$C_{58}BN$	−6.13	−7.92	0.10
$C_{57}BN_2$	−6.66	−8.55	0.16
$C_{56}BN_3$	−6.63	−8.17	0.21

addition of N atoms tends to shift the band gap of $C_{59}B$ above the Fermi level. Compared to others, $C_{56}BN_3$ exhibits the smallest band gap due to increase in the donor states around the Fermi level. The latter phenomenon may modify greatly the surface reactivity of the BN-codoped fullerenes and facilities the charge-transfer between these systems and N_2O molecule.

The dynamic stability of $C_{59-n}BN_n$ fullerenes is also studied by the first-principle molecular dynamic simulations in a period of 2000 fs (2 ps) and at the temperature of 600 K (Fig. S2 of ESI†). It is seen that the cage structure of BN-

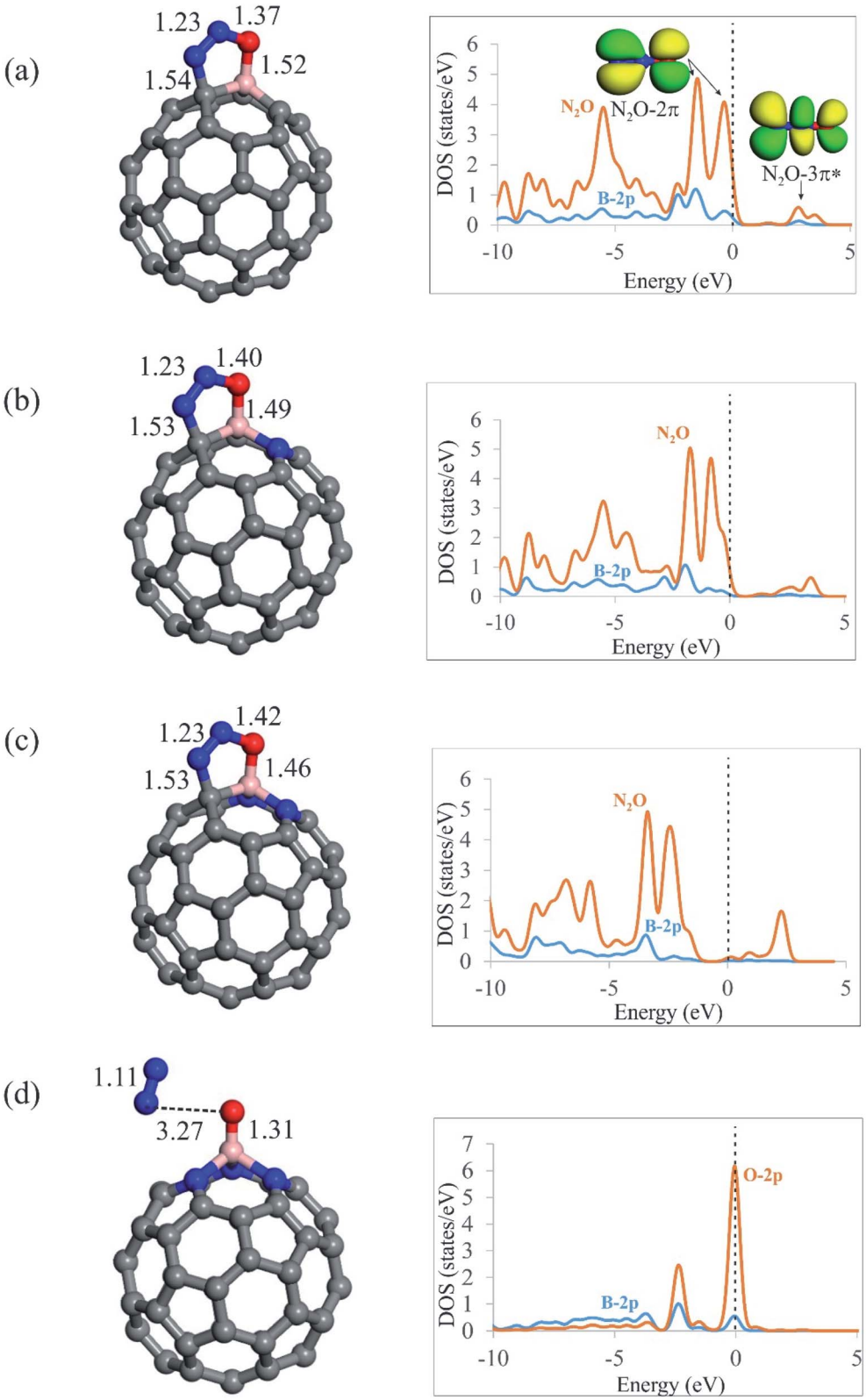

Fig. 2 The optimized local atomic structures, key bond lengths (in Å), and PDOS plots of N_2O adsorbed onto (a) $C_{59}B$, (b) $C_{58}BN$, (c) $C_{57}BN_2$ and (d) $C_{56}BN_3$ fullerenes. In the PDOS plots, the Fermi level is indicated by the dashed line.

codoped fullerenes are almost preserved after the simulations due to strong chemical bonding between the B, C and N atoms. In particular, the lack of any geometry buckling around the B atom suggests that these systems are dynamically stable and therefore can be utilized as a durable and stable catalyst at high temperatures.

Table 2 Adsorption energy (E_{ad}, eV), amount of electron-transfer (Q_{CT}, $|e|$) and Gibbs free energy change (ΔG_{ad}, eV) due to the adsorption of N_2O and CO molecules onto $C_{59-n}BN_n$ fullerenes[a]

	N_2O			CO		
Fullerene	E_{ad}	Q_{CT}	ΔG_{ad}	E_{ad}	Q_{CT}	ΔG_{ad}
$C_{59}B$	−0.54 (−0.53)	0.21 (0.21)	−0.08 (−0.07)	−0.92 (−0.92)	0.24 (0.24)	−0.38 (−0.37)
$C_{58}BN$	−0.62 (−0.60)	0.23 (0.23)	−0.10 (−0.09)	−0.35 (−0.34)	0.21 (0.20)	0.14 (0.15)
$C_{57}BN_2$	−0.70 (−0.68)	0.23 (0.22)	−0.22 (−0.20)	−0.35 (−0.34)	0.22 (0.21)	0.13 (0.14)
$C_{56}BN_3$	−1.95 (−1.93)	0.41 (0.40)	−1.64 (−1.62)	−0.25 (−0.24)	0.20 (0.19)	0.23 (0.23)

[a] The values within the parenthesis refers to the adsorption of N_2O and CO molecules onto endohedral Kr@$C_{59-n}BN_n$ systems.

3.2. N_2O adsorbed configurations

After screening out the surface reactivity and electronic structure of $C_{59-n}BN_n$ fullerenes, we probe the adsorption of N_2O molecule on these systems. Fig. 2 compares the geometry of N_2O molecule adsorbed on the $C_{59-n}BN_n$ fullerenes, and Table 2 summarizes the adsorption energies (E_{ad}), electron-transfer values (Q_{CT}) and Gibbs free energy changes (ΔG_{ad}) due to the adsorption of N_2O. According to earlier studies,[12,84,85] N_2O can be adsorbed on catalyst surfaces *via* three different configurations, namely, linear and [2+2]- or [3+2]-cycloaddition. Our results indicate that the linear configuration, in which N_2O interacts with the B atom of $C_{59-n}BN_n$ fullerenes *via* its N- or O-end is metastable, and it is readily converted into a stable chemisorbed configuration by overcoming a small activation barrier. In the case of $C_{59}B$, $C_{58}BN$ and $C_{57}BN_2$, in which there is at least one carbon atom around the B, the O and N atoms of N_2O bind with the B–C bond through a [3+2]-cycloaddition. From Table 2, the adsorption energies (E_{ad}) of N_2O are calculated to be −0.54, −0.62 and −0.70 eV on $C_{59}B$, $C_{58}BN$ and $C_{57}BN_2$, respectively, indicating that the tendency of fullerenes to adsorb N_2O molecule is improved with the successive incorporation of N atoms. The B–O (N–C) bond distances between N_2O and $C_{59-n}BN_n$ are 1.52 (1.54), 1.49 (1.53) and 1.46 (1.53) Å for $n = 0$, 1 and 2, respectively. This reveals that the interaction between the fullerene and N_2O is enhanced by increasing the N dopants around the B atom. Moreover, the Hirshfeld analysis discloses that the adsorbed N_2O extracts about 0.20 electrons from the fullerene, which occupy its empty $3\pi^*$ orbital, leading to bending of the N–N–O angle. The latter is verified by the PDOS plots in Fig. 2, in which the successive addition of N atoms downshifts the $3\pi^*$ orbital of N_2O. From the Hirshfeld population analysis, the oxygen atom of N_2O is negatively charged by 0.13, 0.15 and 0.16$|e|$ on $C_{59}B$, $C_{58}BN$ and $C_{57}BN_2$, respectively. Besides, the N–O bond length in the free N_2O molecule is 1.19 Å, which is stretched to 1.37, 1.40 and 1.42 Å on $C_{59}B$, $C_{58}BN$ and $C_{57}BN_2$, respectively. These results show that increasing N impurities in $C_{59-n}BN_n$ results in the further activation of N_2O. From Table 2, it is seen that the Gibbs free energy changes (ΔG_{ad}) due to the adsorption of N_2O on $C_{59}B$, $C_{58}BN$ and $C_{57}BN_2$ fullerenes are negative, suggesting the thermodynamic feasibility of this process. Nevertheless, the differences between the E_{ad} and ΔG_{ad} values indicate that the temperature and entropy effects are essential factors, owning to their 0.31–0.52 eV contribution to the adsorption energy.

On the other hand, it is found that the [3+2]-cycloaddition configuration is energetically unfavorable for N_2O on the nitrogen-rich $C_{56}BN_3$ fullerene, since it is spontaneously dissociated into N_2 molecule and an O atom (O*) attached to the B atom (Fig. 2d). It is necessary to state that a similar behavior has been also reported for other surfaces like Si-doped[19] or BN-codoped graphene.[17] As discussed above, the successive introduction of N impurities can largely reinforce the electron-donating property of B-doped fullerene. Hence, one can expect that electron-rich $C_{56}BN_3$ pumps a sizeable electron density to $3\pi^*$ orbital of N_2O, leading to break of its N–O bond. The adsorption energy of N_2O on $C_{56}BN_3$ is −1.95 eV, which indicates that the dissociation of this molecule is energetically favorable. Also, this implies that the O* atom is tightly attached to B atom. The Hirshfeld analysis discloses that the O atom adsorbed on the B atom is negatively charged by about 0.40$|e|$, which suggests its efficient electron donating property. Like other BN-codoped fullerenes as discussed above, the negative ΔG_{ad} value for the N_2O adsorption on $C_{56}BN_3$ indicates that it is a thermodynamically facile process at ambient temperature mainly due to the increase of entropy. Considering the PDOS plot in Fig. 2d, it is observed that the O-2p

Table 3 Electron density (ρ_{BCP}, a.u.), its Laplacian ($\nabla^2\rho_{BCP}$, a.u.) and total electronic energy density (H_{BCP}, a.u.) at the B–N BCPs of N_2O adsorbed and B–C BCPs of CO adsorbed $C_{59-n}BN_n$ complexes

	N_2O			CO		
Fullerene	ρ_{BCP}	$\nabla^2\rho_{BCP}$	H_{BCP}	ρ_{BCP}	$\nabla^2\rho_{BCP}$	H_{BCP}
$C_{59}B$	−0.54 (−0.53)	0.21 (0.21)	−0.08 (−0.07)	−0.92 (−0.92)	0.24 (0.24)	−0.38 (−0.37)
$C_{58}BN$	−0.62 (−0.60)	0.23 (0.23)	−0.10 (−0.09)	−0.35 (−0.34)	0.21 (0.20)	0.14 (0.15)
$C_{57}BN_2$	−0.70 (−0.68)	0.23 (0.22)	−0.22 (−0.20)	−0.35 (−0.34)	0.22 (0.21)	0.13 (0.14)
$C_{56}BN_3$	−1.95 (−1.93)	0.41 (0.40)	−1.64 (−1.62)	−0.25 (−0.24)	0.20 (0.19)	0.23 (0.23)

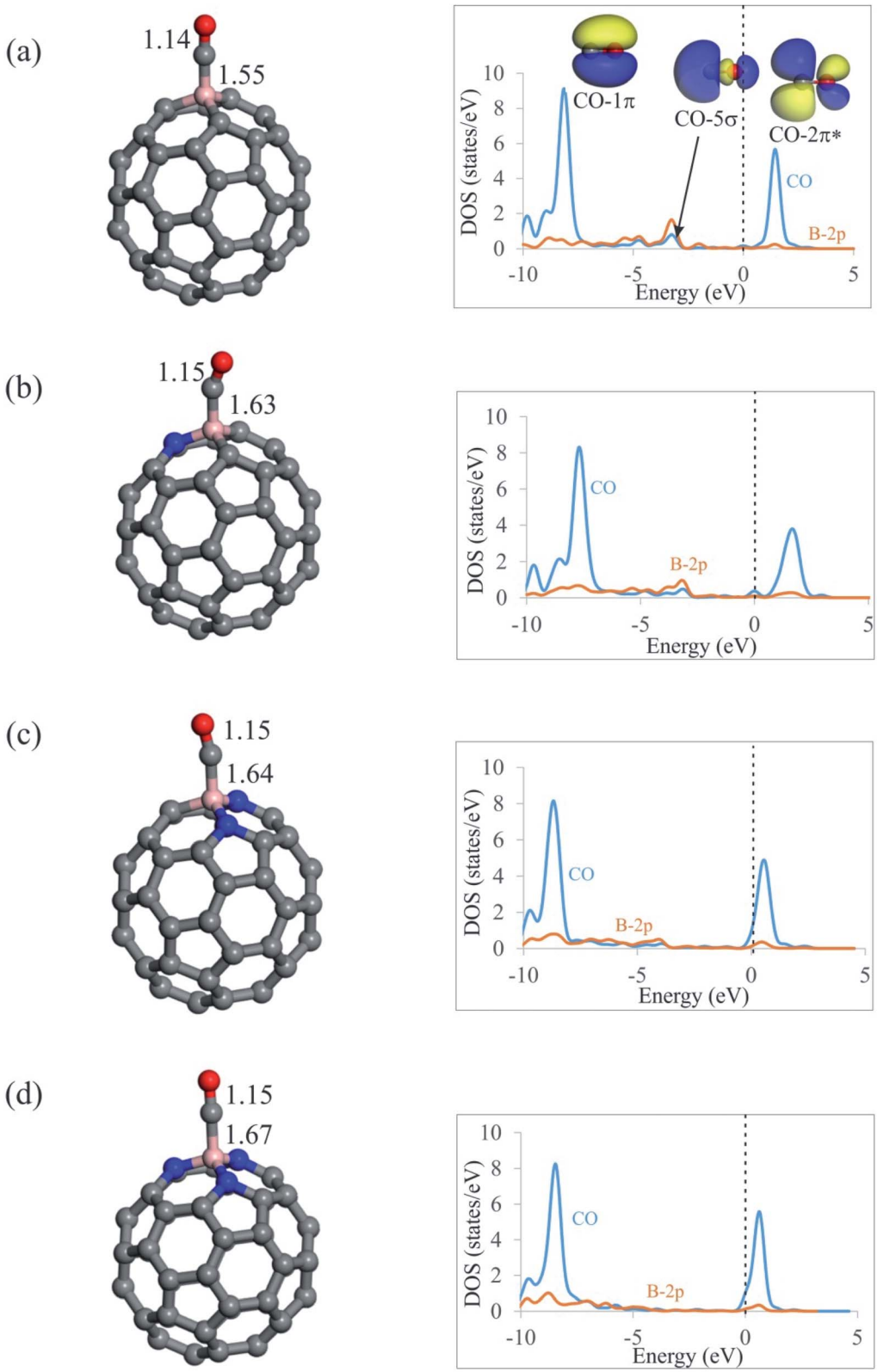

Fig. 3 The optimized local atomic structures, binding distances (in Å), and PDOS plots of CO adsorbed onto (a) $C_{59}B$, (b) $C_{58}BN$, (c) $C_{57}BN_2$ and (d) $C_{56}BN_3$ fullerenes. In the PDOS plots, the Fermi level is indicated by the dashed line.

states are favorably coupled with the B-2p states at the Fermi level. This observation agrees well with the calculated E_{ad} and ΔG_{ad} values, implying that the O* is strongly adsorbed on the B atom.

As noted before, one of the key questions that has inspired this study is the effect of encapsulating a Ng atom on the catalytic activities of the $C_{59-n}BN_n$ fullerenes. To achieve this

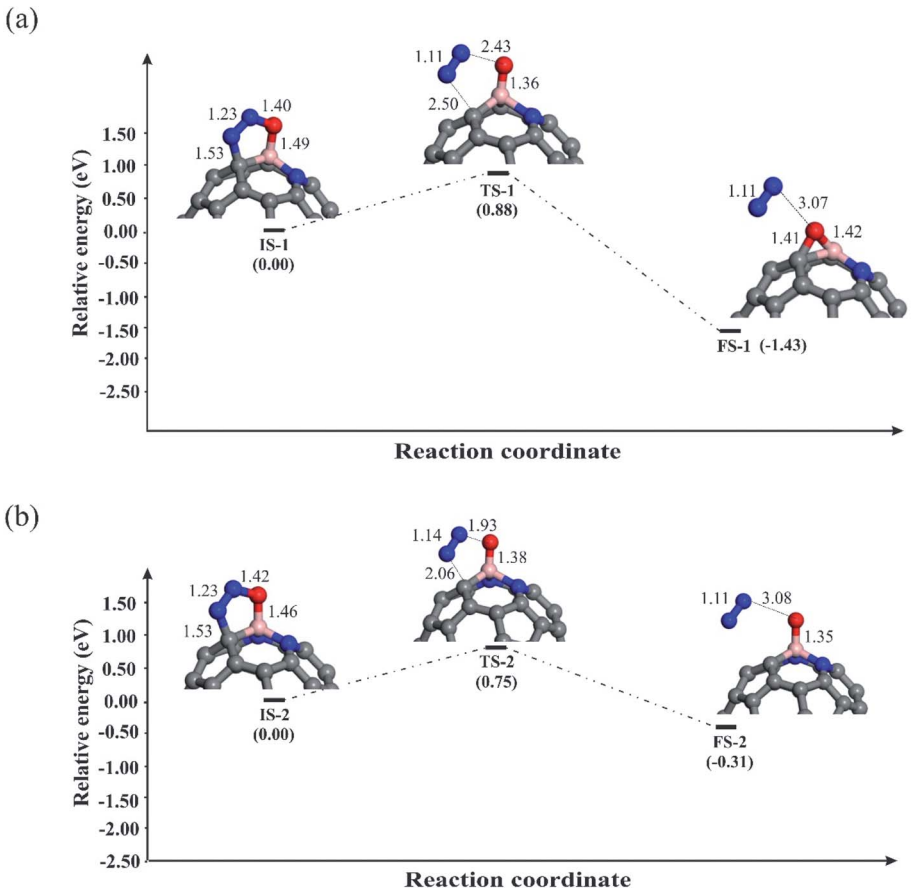

Fig. 4 The potential energy diagram and relevant bond distances (in Å) for direct decomposition of N_2O over (a) $C_{58}BN$ and (b) $C_{57}BN_2$ fullerenes.

goal, a Kr atom was put in the center of the fullerenes, and the N_2O adsorption was then studied over the resulting systems (Fig. S3†). The B–O bond lengths between encapsulated fullerenes and N_2O molecule range from 1.31 to 1.52 Å, which is nearly equal to those reported for empty $C_{59-n}BN_n$ systems. The Kr atom is stably inserted within the $C_{59-n}BN_n$ fullerenes in all studied systems due to its negative adsorption energy (≈ -0.54 eV). Meanwhile, following encapsulation, the Kr atom obtains a positive charge of $0.25|e|$, suggesting that the Kr atom redistributes the electron density within the fullerene. As a result, the N_2O adsorption energies on $Kr@C_{59-n}BN_n$ fullerenes are slightly lower than those on empty $C_{59-n}BN_n$ fullerenes. It is also worth noting that the Kr encapsulation has no effect on the order of the N_2O adsorption energies on $C_{59-n}BN_n$ fullerenes. These findings support previous findings[68] that adding a noble gas into C_{60} has little effect on its surface reactivity and hence catalytic properties.

The calculated ρ_{BCP}, $\nabla^2\rho_{BCP}$ and H_{BCP} values associated with the B–O BCPs of N_2O adsorbed complexes are shown in Table 3. It is seen that the ρ_{BCP} value at the B–O BCPs increases as the number of the N atoms increases, which is consistent with the adsorption energies discussed above. However, the $\nabla^2\rho_{BCP}$ values at these BCPs are all positive, but the H_{BCP} values are all negative, suggesting that the B–O bonds in these systems are partly covalent. Importantly, the associated H_{BCP} values vary as $C_{56}BN_3 > C_{57}BN_2 > C_{58}BN > C_{59}B$, showing that the degree of covalency in the B–O bonds increases with the number of doped N atoms.

3.3. CO adsorbed configurations

From Fig. 3, it is seen that CO molecule prefers to interact with the B atom of $C_{59-n}BN_n$ fullerenes *via* its C atom. The E_{ad} of CO on $C_{59}B$ is -0.92 eV, which agrees well with those reported by other DFT studies.[58] Meanwhile, this quite large negative value indicates the chemisorption nature of the adsorption. On the contrary, our results in Table 2 show that tendency of $C_{59-n}BN_n$ fullerenes to capture CO molecule decreases with the addition of N atoms around the B atom. In particular, the E_{ad} value of CO on nitrogen rich $C_{56}BN_3$ structure is -0.25 eV, which demonstrates the physisorption of this molecule. Besides, the binding distances between the fullerenes and C atom of CO are 1.55, 1.63, 1.64 and 1.67 Å for $C_{59}B$, $C_{58}BN$, $C_{57}BN_2$ and $C_{56}BN_3$, respectively, indicating that the CO interaction with the B atom is weakened with the increasing the content of N dopants. Note that the order of E_{ad} values of CO on $C_{59-n}BN_n$ is not correlated with the positive charges on the B atom or MEP analysis results. This may suggest that the electrostatic interaction between the B atom and CO has a negligible contribution in the resulting complexes. Moreover, the values of ΔG_{ad} in Table 2 indicate that unlike $C_{59}B$, the CO adsorption would not be thermodynamically

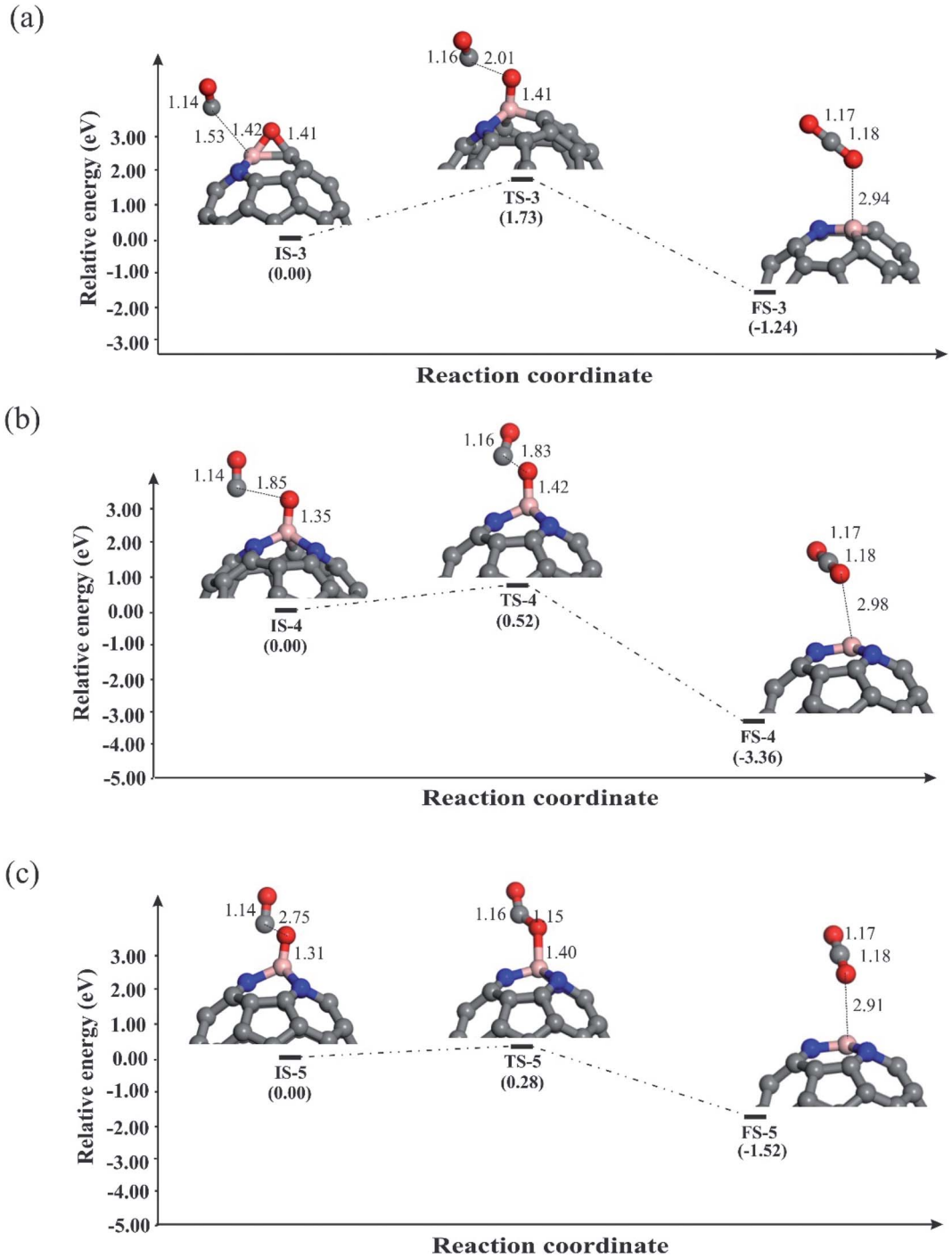

Fig. 5 The potential energy diagram and relevant bond distances (in Å) for removing O* atom by CO over (a) $C_{58}BN$, (b) $C_{57}BN_2$ and (c) $C_{56}BN_3$ fullerenes.

possible at room temperature. According to Table 2, the CO adsorption is associated with a charge-transfer from CO molecule into fullerene with the values in the range of 0.20–0.24|e|. Considering the PDOS plots in Fig. 3, one can see that there is a noticeable interaction between the CO-5σ and the vacant B-2p states below the Fermi level especially for the $C_{59}B$ system. Also, a weak orbital interaction occurs between CO-2π* and B atom, which accounts for the lengthening of C–O bond in these systems.

Table 2 shows that adding a Kr atom to the $C_{59-n}BN_n$ fullerenes has little or no influence on the E_{ad}, Q_{CT} and ΔG_{ad} values of CO molecule. That is, with the exception of Kr@$C_{59}B$, CO adsorption is still weak and belongs to physisorption. Furthermore, the calculated ρ_{BCP} values show that, among the $C_{59-n}BN_n$ fullerenes studied, $C_{56}BN_3$ forms the weakest complex with the CO molecule (Table 3). Also, the positive $\nabla^2\rho_{BCP}$ and negative H_{BCP} values at the B–C BCPs indicate that

these bonds are partly covalent. The H_{BCP} values in Table 3 show that, with the exception of $C_{59}B$ complexes, the B–N bonds in the N_2O adsorbed complexes are more covalent than the B–C bonds in the CO adsorbed systems.

The above findings clearly demonstrate that increasing the N coordination to the B atom of $C_{59}B$ would be beneficial for N_2O capture, which is the starting point for the N_2O reduction process. The surrounding B–N bonds, in particular, make $C_{56}BN_3$ an effective catalyst for the spontaneous decomposition of N_2O. More importantly, BN-codoped fullerenes have a lower capacity to trap CO molecules than $C_{59}B$, suggesting that they should be extremely resistant to CO poisoning. As a result, BN-codoped fullerenes appear to have excellent catalytic activity in the reduction of N_2O. The N_2O reduction on the $C_{59-n}BN_n$ systems is compared in detail in the next section.

3.4. N_2O reduction

Now we explore the possible reduction mechanisms for reduction of N_2O on BN-codoped fullerenes ($C_{58}BN$, $C_{57}BN_2$ and $C_{56}BN_3$). Based on the earlier investigations,[86] depending on the order of adsorption energies of N_2O and CO on the catalyst, N_2O reduction can proceed *via* two main pathways, *i.e.*, the Eley–Rideal (E–R) and Langmuir–Hinshelwood (L–H). In the E–R mechanism, which is also known as the stepwise pathway, a N_2O molecule is initially adsorbed and decomposed on the catalyst and then a CO molecule interacts with the remaining O* species to generate CO_2 molecule. In contrast, the L–H or concerted mechanism involves the simultaneous binding of N_2O and CO molecules to the catalyst. Both these mechanisms are investigated here to realize the most energetically favorable pathway of N_2O reduction. The relaxed atomic structures and energy profiles of these competing pathways are given in Fig. 4–6.

Let us first discuss the E–R mechanism for the N_2O reduction reaction on the BN-codoped fullerenes. As discussed above, N_2O is adsorbed on the $C_{58}BN$ and $C_{57}BN_2$ fullerenes *via* a [3+2]-cycloaddition, while it is spontaneously decomposed on $C_{56}BN_3$. This suggests that the first step of the N_2O reduction is already completed on the latter system and hence we only focus on the N_2O decomposition mechanism on $C_{58}BN$ and $C_{57}BN_2$. Fig. 4a and b indicate the reaction pathways for the $N_2O \rightarrow N_2 + O^*$ elementary reaction on $C_{58}BN$ and $C_{57}BN_2$, respectively. To start the reaction, N–O bond of the adsorbed N_2O is elongated and the negative charge on the O* atom is continuously increased. Passing over the transition states TS-1 and TS-2 with an activation barrier (E_{bar}) of 0.88 and 0.75 eV, respectively, N_2O

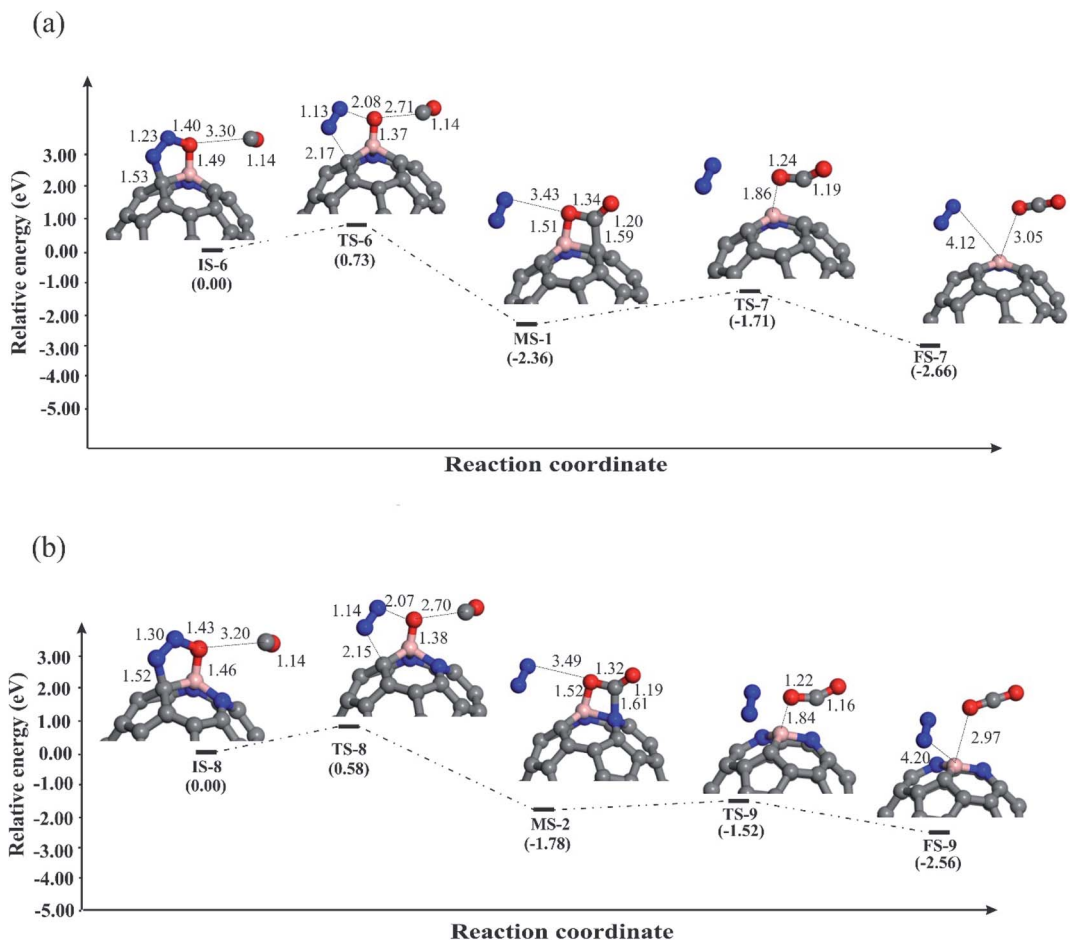

Fig. 6 The potential energy diagram and relevant bond distances (in Å) for reduction of N_2O by CO molecule through the L–H mechanism over (a) $C_{58}BN$ and (b) $C_{57}BN_2$ fullerenes.

is decomposed on the $C_{58}BN$ and $C_{57}BN_2$. At the final state, the O atom is attached on the B atom, while N_2 molecule is separated from the fullerene with a binding distance of ≈3 Å. An interesting finding here is that the E_{bar} for the decomposition of N_2O varies with the positive charge on the B atom. That is, the E_{bar} values for the decomposition of N_2O on $C_{57}BN_2$ fullerenes is less than the corresponding value obtained for the $C_{58}BN$, confirming that the catalytic performance of the fullerene is improved with the addition of N atoms around the B. Besides, these E_{bar} values are less than the reported value for the noble-metal based Ag_7Au_6 catalyst (1.1 eV).[87] It should point out that unlike $C_{57}BN_2$, the O* moiety resulting from the N_2O decomposition is strongly chemisorbed on the B–C bond of $C_{58}BN$ through the formation of an epoxide-like structure. Note that a similar species has been also found on the $C_{59}B$ structure,[34] suggesting that $C_{58}BN$ is readily oxidized during the N_2O reduction process.

To complete the catalytic cycle, the remaining O* should be removed by CO molecule. To examine the energy profile, we added the CO molecule on the O* to form the corresponding initial state (Fig. 5). Next, CO approaches the O* and by passing the corresponding transition state, the CO_2 molecule is achieved. Like $C_{59}B$,[34] the E_{bar} value for the removing O* on $C_{58}BN$ is relatively high (1.73 eV), owning to the strong adsorption of this species on the B–C bond. On the contrary, the energy barrier for the $CO + O^* \rightarrow CO_2$ on $C_{57}BN_2$ and $C_{56}BN_3$ fullerenes are 0.52 and 0.28 eV, respectively, which are small enough to be easily overcome at normal temperatures. The CO_2 is finally separated from the fullerenes, and this restores the catalyst to begin a new N_2O reduction process.

We further explored the N_2O reduction process through the L–H mechanism, in which N_2O and CO molecules are first coadsorbed on fullerenes. Fig. 6 depicts the obtained geometric structures for involved species in this mechanism. The shortest binding distance between N_2O and CO in the initial state (IS-6 and IS-8) is about 3 Å, hinting at the weak nature of the interaction between them. Then, CO moves towards the N_2O until a stable OCO intermediate is obtained on the fullerene. Though this reaction step is exothermic on both BN-codoped structures, the energy barriers and the reaction energies are not similar. An interesting finding is that the energy barrier to obtain the OCO species decreases as the nitrogen content around the B atom increases. Due to large activation of N_2O on the $C_{57}BN_2$, a relatively smaller E_{bar} is obtained (0.36 eV), which is comparable to the mentioned value for the Fe-doped graphene (0.83 eV).[86] Also, these E_{bar} values are lower than that of over $C_{59}B$ (1.95 eV),[88] suggesting that the BN codoping is able to substantially improve the catalytic properties of the C_{60} fullerene. In the next step, the OCO is converted to CO_2 molecule as shown in Fig. 6. This elementary reaction is also exothermic but requests an activation barrier of 0.73 ($C_{58}BN$) and 0.58 eV ($C_{57}BN_2$), which seems to be easily provided at room temperature. The resulting CO_2 molecule has a small E_{ad} value, so it can be simply separated from the active site of the fullerenes.

4. Conclusions

We used dispersion-corrected DFT calculations to explore the catalytic and electronic structure properties of BN-codoped C_{60} fullerenes. The results showed that by successively doping N atoms around the B in $C_{59}B$, the tendency of the fullerene to interact with N_2O molecule increases. The B atom in $C_{56}BN_3$ acts as an efficient catalytic site for the spontaneous decomposition of N_2O because the surrounding B–N bonds hinder the formation of secondary C–N bond between the fullerene and N_2O. Furthermore, the fact that BN-codoped fullerenes have a low tendency for capturing CO molecule implies that they are tolerant to CO poisoning. The adsorption energies of N_2O and CO are not influenced by the introduction of a Kr atom inside the $C_{59-n}BN_n$ fullerenes. The activation barriers for N_2O reduction *via* the L–H mechanism are lower than those for the E–R mechanism over $C_{57}BN_2$ and $C_{56}BN_3$, indicating that this reaction would occur *via* the former pathway. Even though that N_2O reduction is exothermic over the $C_{59-n}BN_n$ fullerenes, the obtained activation barriers vary with number of nitrogen atoms in these systems. Nitrogen dopants surrounding the B atom, for example, inhibit the poisoning of $C_{57}BN_2$ and $C_{56}BN_3$ fullerenes by the O* moiety. The nitrogen-rich $C_{56}BN_3$ fullerene has the highest catalytic activity for N_2O reduction due to its unique electronic structure and charge-transfer. We hope that this new understanding will inspire the development of highly efficient metal-free catalysts based on carbon fullerenes, as well as provide a theoretical basis for future studies into the removal of hazardous N_2O and CO pollutants from the environment.

Conflicts of interest

There are no conflicts to declare.

References

1 S. A. Montzka, E. J. Dlugokencky and J. H. Butler, *Nature*, 2011, **476**, 43–50.
2 A. Tatar, A. Barati-Harooni, A. Najafi-Marghmaleki, A. Mohebbi, M. M. Ghiasi, A. H. Mohammadi and A. Hajinezhad, *Int. J. Greenhouse Gas Control*, 2016, **49**, 47–54.
3 D. J. Wuebbles, *Science*, 2009, **326**, 56–57.
4 R. Portmann, J. Daniel and A. Ravishankara, *Philos. Trans. R. Soc., B*, 2012, **367**, 1256–1264.
5 J.-D. Lee, W.-P. Fang, C.-S. Li and C.-H. Cheng, *J. Chem. Soc., Dalton Trans.*, 1991, 1923–1927.
6 J. A. Ryder, A. K. Chakraborty and A. T. Bell, *J. Phys. Chem. B*, 2002, **106**, 7059–7064.
7 P. Pannopard, P. Khongpracha, C. Warakulwit, S. Namuangruk, M. Probst and J. Limtrakul, *ChemPhysChem*, 2012, **13**, 583–587.
8 J. s. A. Luque-Urrutia and A. Poater, *Inorg. Chem.*, 2017, **56**, 14383–14387.
9 A. Heyden, B. Peters, A. T. Bell and F. J. Keil, *J. Phys. Chem. B*, 2005, **109**, 1857–1873.
10 A. Heyden, N. Hansen, A. T. Bell and F. J. Keil, *J. Phys. Chem. B*, 2006, **110**, 17096–17114.
11 E. Pachatouridou, E. Papista, E. F. Iliopoulou, A. Delimitis, G. Goula, I. V. Yentekakis, G. E. Marnellos and M. Konsolakis, *J. Environ. Chem. Eng.*, 2015, **3**, 815–821.

12 A. L. Yakovlev, G. M. Zhidomirov and R. A. van Santen, *Catal. Lett.*, 2001, **75**, 45–48.
13 V. Blagojevic, G. Orlova and D. K. Bohme, *J. Am. Chem. Soc.*, 2005, **127**, 3545–3555.
14 S. M. Hamilton, W. S. Hopkins, D. J. Harding, T. R. Walsh, P. Gruene, M. Haertelt, A. Fielicke, G. Meijer and S. R. Mackenzie, *J. Am. Chem. Soc.*, 2010, **132**, 1448–1449.
15 G. Walther, D. J. Mowbray, T. Jiang, G. Jones, S. Jensen, U. J. Quaade and S. Horch, *J. Catal.*, 2008, **260**, 86–92.
16 S. Pornsatitworakul, S. Phikulthai, S. Namuangruk and B. Boekfa, *Int. Conference on IEEE*, 2015, pp. 225–229.
17 M. D. Esrafili, *Chem. Phys. Lett.*, 2018, **705**, 44–49.
18 M. D. Esrafili, F. Mohammadian-Sabet and P. Nematollahi, *RSC Adv.*, 2016, **6**, 64832–64840.
19 J.-X. Zhao, Y. Chen and H.-G. Fu, *Theor. Chem. Acc.*, 2012, **131**, 1242.
20 A. Junkaew, S. Namuangruk, P. Maitarad and M. Ehara, *RSC Adv.*, 2018, **8**, 22322–22330.
21 N. Martin, M. Altable, S. Filippone and A. Martin-Domenech, *Synlett*, 2007, **2007**, 3077–3095.
22 B. C. Thompson and J. M. Fréchet, *Angew. Chem., Int. Ed.*, 2008, **47**, 58–77.
23 A. K. Geim, *Science*, 2009, **324**, 1530–1534.
24 B. F. Machado and P. Serp, *Catal. Sci. Technol.*, 2012, **2**, 54–75.
25 P. Lazar, F. e. Karlický, P. Jurečka, M. s. Kocman, E. Otyepková, K. r. Šafářová and M. Otyepka, *J. Am. Chem. Soc.*, 2013, **135**, 6372–6377.
26 Y. García-Rodeja, M. Solà and I. Fernández, *J. Org. Chem.*, 2016, **82**, 754–758.
27 K. Kakaei, M. D. Esrafili and A. Ehsani, in *Interface Science and Technology*, ed. K. Kakaei, M. D. Esrafili and A. Ehsani, Elsevier, 2019, vol. 27, pp. 339–386.
28 T. Wehling, K. Novoselov, S. Morozov, E. Vdovin, M. Katsnelson, A. Geim and A. Lichtenstein, *Nano Lett.*, 2008, **8**, 173–177.
29 X. Wang, X. Li, L. Zhang, Y. Yoon, P. K. Weber, H. Wang, J. Guo and H. Dai, *Science*, 2009, **324**, 768–771.
30 B. Guo, L. Fang, B. Zhang and J. R. Gong, *Insci. J.*, 2011, 80–89.
31 M. D. Esrafili and P. Mousavian, *Appl. Surf. Sci.*, 2018, **455**, 808–814.
32 Q. Z. Li, J. J. Zheng, J. S. Dang and X. Zhao, *ChemPhysChem*, 2015, **16**, 390–395.
33 M. D. Esrafili and S. Heidari, *Comput. Theor. Chem.*, 2019, **11**, 50–57.
34 K.-Y. Chen, S.-Y. Wu and H.-T. Chen, *ACS Omega*, 2020, **5**, 28870–28876.
35 F. Gao, G. L. Zhao, S. Yang and J. J. Spivey, *J. Am. Chem. Soc.*, 2013, **135**, 3315–3318.
36 H. Wang, M. Xie, L. Thia, A. Fisher and X. Wang, *J. Phys. Chem. Lett.*, 2014, **5**, 119–125.
37 D. C. Camacho-Mojica, E. Muñoz-Sandoval and F. López-Urías, *Carbon*, 2017, **116**, 381–390.
38 Z. Xie, M. Chen, S. G. Peera, C. Liu, H. Yang, X. Qi, U. P. Kumar and T. Liang, *ACS Omega*, 2020, **5**, 5142–5149.
39 K. Gong, F. Du, Z. Xia, M. Durstock and L. Dai, *Science*, 2009, **323**, 760–764.
40 Y. Feng, F. Li, Z. Hu, X. Luo, L. Zhang, X.-F. Zhou, H.-T. Wang, J.-J. Xu and E. Wang, *Phys. Rev. B: Condens. Matter Mater. Phys.*, 2012, **85**, 155454.
41 H. Miao, S. Li, Z. Wang, S. Sun, M. Kuang, Z. Liu and J. Yuan, *Int. J. Hydrogen Energy*, 2017, **42**, 28298–28308.
42 R. Shi, J. Zhao, S. Liu, W. Sun, H. Li, P. Hao, Z. Li and J. Ren, *Carbon*, 2018, **130**, 185–195.
43 L. Yu, X. Pan, X. Cao, P. Hu and X. Bao, *J. Catal.*, 2011, **282**, 183–190.
44 P. Zhang, J. S. Lian and Q. Jiang, *Phys. Chem. Chem. Phys.*, 2012, **14**, 11715–11723.
45 F. Studt, *Catal. Lett.*, 2013, **143**, 58–60.
46 Y. Tang, W. Chen, Z. Shen, S. Chang, M. Zhao and X. Dai, *Carbon*, 2017, **111**, 448–458.
47 M. D. Esrafili and S. Asadollahi, *Appl. Surf. Sci.*, 2018, **463**, 526–534.
48 X. Liu, Y. Sui, T. Duan, C. Meng and Y. Han, *Catal. Sci. Technol.*, 2015, **5**, 1658–1667.
49 X. Zhang, Z. Lu, Y. Tang, Z. Fu, D. Ma and Z. Yang, *Phys. Chem. Chem. Phys.*, 2014, **16**, 20561–20569.
50 L. Ferrighi, M. I. Trioni and C. Di Valentin, *J. Phys. Chem. C*, 2015, **119**, 6056–6064.
51 L. Qin, L. Wang, X. Yang, R. Ding, Z. Zheng, X. Chen and B. Lv, *J. Catal.*, 2018, **359**, 242–250.
52 S. Wang, J. Feng, Q. Meng, B. Cao and G. Tian, *J. Solid State Electrochem.*, 2019, **23**, 2377–2390.
53 M. D. Esrafili and H. Janebi, *Mol. Phys.*, 2020, **118**, e1631495.
54 S. Wang, L. Zhang, Z. Xia, A. Roy, D. W. Chang, J. B. Baek and L. Dai, *Angew. Chem., Int. Ed.*, 2012, **51**, 4209–4212.
55 Y. Zheng, Y. Jiao, L. Ge, M. Jaroniec and S. Z. Qiao, *Angew. Chem.*, 2013, **125**, 3192–3198.
56 J.-i. Ozaki, T. Anahara, N. Kimura and A. Oya, *Carbon*, 2006, **44**, 3358–3361.
57 J.-i. Ozaki, N. Kimura, T. Anahara and A. Oya, *Carbon*, 2007, **45**, 1847–1853.
58 B. Gao and G. Chen, *RSC Adv.*, 2019, **9**, 21626–21636.
59 Y.-X. Yu, *Phys. Chem. Chem. Phys.*, 2013, **15**, 16819–16827.
60 H. Jiang, T. Zhao, L. Shi, P. Tan and L. An, *J. Phys. Chem. C*, 2016, **120**, 6612–6618.
61 S. Nachimuthu, P.-J. Lai and J.-C. Jiang, *Carbon*, 2014, **73**, 132–140.
62 S. Guha and K. Nakamoto, *Coord. Chem. Rev.*, 2005, **249**, 1111–1132.
63 A. Takeda, Y. Yokoyama, S. Ito, T. Miyazaki, H. Shimotani, K. Yakigaya, T. Kakiuchi, H. Sawa, H. Takagi and K. Kitazawa, *Chem. Commun.*, 2006, 912–914.
64 R. B. Ross, C. M. Cardona, D. M. Guldi, S. G. Sankaranarayanan, M. O. Reese, N. Kopidakis, J. Peet, B. Walker, G. C. Bazan and E. Van Keuren, *Nat. Mater.*, 2009, **8**, 208–212.
65 A. A. Popov, S. Yang and L. Dunsch, *Chem. Rev.*, 2013, **113**, 5989–6113.
66 F. Cimpoesu, S. Ito, H. Shimotani, H. Takagi and N. Dragoe, *Phys. Chem. Chem. Phys.*, 2011, **13**, 9609–9615.

67 M. Bühl, S. Patchkovskii and W. Thiel, *Chem. Phys. Lett.*, 1997, **275**, 14–18.
68 S. Osuna, M. Swart and M. Sola, *Phys. Chem. Chem. Phys.*, 2011, **13**, 3585–3603.
69 A. Bil and C. A. Morrison, *J. Phys. Chem. A*, 2012, **116**, 3413–3419.
70 J. P. Perdew, K. Burke and M. Ernzerhof, *Phys. Rev. Lett.*, 1996, **77**, 3865–3868.
71 S. Grimme, *J. Comput. Chem.*, 2006, **27**, 1787–1799.
72 B. Delley, *J. Chem. Phys.*, 1990, **92**, 508–517.
73 B. Delley, *J. Chem. Phys.*, 2000, **113**, 7756–7764.
74 C. O. Ulloa, M. Ponce-Vargas and A. Munoz-Castro, *J. Phys. Chem. C*, 2018, **122**, 25110–25117.
75 J. C. Gonzalez, S. Mondal, F. Ocayo, R. Guajardo-Maturana and A. Muñoz-Castro, *Int. J. Quantum Chem.*, 2020, **120**, e26080.
76 R. Bader, *Atoms in Molecules: A Quantum Theory*, Clarendon Press, Oxford, 1990.
77 I. Rozas, I. Alkorta and J. Elguero, *J. Am. Chem. Soc.*, 2000, **122**, 11154–11161.
78 F. Biegler-König and J. Schönbohm, *J. Comput. Chem.*, 2002, **23**, 1489–1494.
79 M. J. Frisch, G. W. Trucks, H. B. Schlegel, G. E. Scuseria, M. A. Robb, J. R. Cheeseman, G. Scalmani, V. Barone, G. A. Petersson, H. Nakatsuji, X. Li, M. Caricato, A. Marenich, J. Bloino, B. G. Janesko, R. Gomperts, B. Mennucci, H. P. Hratchian, J. V. Ortiz, A. F. Izmaylov, J. L. Sonnenberg, D. Williams-Young, F. Ding, F. Lipparini, F. Egidi, J. Goings, B. Peng, A. Petrone, T. Henderson, D. Ranasinghe, V. G. Zakrzewski, J. Gao, N. Rega, G. Zheng, W. Liang, M. Hada, M. Ehara, K. Toyota, R. Fukuda, J. Hasegawa, M. Ishida, T. Nakajima, Y. Honda, O. Kitao, H. Nakai, T. Vreven, K. Throssell, J. A. Montgomery Jr, J. E. Peralta, F. Ogliaro, M. Bearpark, J. J. Heyd, E. Brothers, K. N. Kudin, V. N. Staroverov, T. Keith, R. Kobayashi, J. Normand, K. Raghavachari, A. Rendell, J. C. Burant, S. S. Iyengar, J. Tomasi, M. Cossi, J. M. Millam, M. Klene, C. Adamo, R. Cammi, J. W. Ochterski, R. L. Martin, K. Morokuma, O. Farkas, J. B. Foresman, and D. J. Fox, *Gaussian 09, Revision A.02*, Gaussian, Inc., Wallingford CT, 2016.
80 Y. Wang, M. Jiao, W. Song and Z. Wu, *Carbon*, 2017, **114**, 393–401.
81 M. D. Esrafili and N. Mohammadirad, *Mol. Phys.*, 2017, **115**, 1633–1641.
82 C. Ramachandran, *J. Phys. Chem. A*, 2017, **121**, 1708–1714.
83 R. Sanderson, *Chemical Bonds and Bonds Energy*, Elsevier, 2012.
84 A. L. Yakovlev, G. M. Zhidomirov and R. A. van Santen, *J. Phys. Chem. B*, 2001, **105**, 12297–12302.
85 P. Nematollahi and M. D. Esrafili, *RSC Adv.*, 2016, **6**, 59091–59099.
86 S. Wannakao, T. Nongnual, P. Khongpracha, T. Maihom and J. Limtrakul, *J. Phys. Chem. C*, 2012, **116**, 16992–16998.
87 S. T. Oyama, *Mechanisms in Homogeneous and Heterogeneous Epoxidation Catalysis*, Elsevier, 2011.
88 M. D. Esrafili and S. Heydari, *ChemistrySelect*, 2019, **4**, 2267–2274.